A New Chromium-Free Welding Consumable for Joining Austenitic Stainless Steels

A novel Ni-Cu-based consumable was developed to reduce Cr(VI) in the fume generated during welding of Type 304L stainless steel

BY J. W. SOWARDS, D. LIANG, B. T. ALEXANDROV, G. S. FRANKEL, AND J. C. LIPPOLD

ABSTRACT

Federal legislation was enacted in 2006 reducing the permissible exposure limit (PEL) of workers, including welding-related personnel, to Cr(VI) by an order of magnitude. Achieving the new level may not always be practical during fabrication or repair of stainless components in tightly enclosed locations. Therefore, the current study was performed to evaluate the use of Ni-Cu-based welding consumables to weld Type 304L stainless steel while achieving significant reductions of Cr(VI) bearing compounds in welding fume. Consumables were made in bare wire form for gas tungsten arc welding (GTAW) and in coated form for shielded metal arc welding (SMAW). During the development of these consumables, several generations were produced with each improving on the previous generation. Weldability was a primary focus during the development process because switching from a stainless steel welding consumable to a Ni-based alloy could potentially exacerbate weldability issues such as solidification, liquation, and ductility dip cracking. Welds were deposited on Type 304L base metal with the consumables developed during the study and subjected to various tests to evaluate mechanical and corrosion behavior, resistance to weld cracking issues typical of Ni-based alloys, and fume generation characteristics. Weld mechanical properties and weldability performance were similar in nature to other austenitic Ni-based alloys and stainless steels. By using the Ni-Cu based consumable to weld stainless steel, Cr(VI) in the welding fume was reduced by two orders of magnitude from conventional stainless steel welding electrodes.

Introduction

Environmental and occupational safety awareness is becoming increasingly important in today's workplace. This is impacting the welding industry because government standards are decreasing the allowable levels of certain elements and species present in welding fume (Ref. 1). Cr is typically found in stainless steel welding fume because it is one of the major alloying additions used in such consumables. Welding fume generated during stainless steel welding has been shown to contain compounds such as CrO_3, Na_2CrO_4, and K_2CrO_4, which contain Cr in its hexavalent state, i.e., Cr(VI) (Refs. 2–4). Since at least the mid 1970s, United States government agencies such as the National Institute for Occupational Safety and Health (NIOSH) have labeled Cr(VI) compounds as suspected carcinogens (Ref. 5). Starting in 1988, the Occupational Safety and Health Administration (OSHA) began to consider all Cr(VI) compounds as potential carcinogens (Ref. 6). Most recently in 2006, OSHA released its latest ruling that drastically reduced the permissible exposure limit (PEL) of Cr(VI) compounds in the vicinity of welding personnel from 52 to 5 $\mu g\ m^{-3}$. This ruling is a result of their findings that workers are at an elevated risk of developing lung cancer and asthma, as well as nasal and skin damage due to Cr(VI) exposure. The exposure level for total welding fume prior to 1989 was set at 5 $mg\ m^{-3}$ over an 8-h work day (Ref. 7). This limit was abandoned after 1989 and no longer became enforceable since the composition of welding fume was deemed to vary too widely, and because of possible interactions between various constituents in the fume.

J. W. SOWARDS (jeffrey.sowards@nist.gov) *was formerly with, and B. T. ALEXANDROV and J. C. LIPPOLD are currently with the Welding & Joining Metallurgy Group, The Ohio State University, Columbus, Ohio. D. LIANG was formerly with, and G. S. FRANKEL is currently with the Fontana Corrosion Center, The Ohio State University.*

KEYWORDS

Cr(VI)
Ni-Cu
Type 304L
GTAW,
SMAW
Permissible Exposure Limit
Generation I, II, III, and IV Consumables

With regard to Cr(VI) fume control, in particular, several options have been suggested to remediate overexposure once it has been found that the PEL is exceeded (Ref. 8). The welding process may be changed from a process that uses alkali metals in the flux to a bare wire process. The presence of alkali metals can greatly increase Cr(VI) formation and have higher inherent fume generation rates. Changing shielding gasses or making welding parameter adjustments may also reduce fume generation rates. In addition to process modifications, some research has suggested compositional modifications. Zn additions made to metal cored stainless steel wires showed that Zn preferentially reacts with available oxygen during fume formation, thus reducing the oxidation of chromium, but with increased fume generation rates (Ref. 9). The replacement of potassium with lithium was also performed demonstrating the reduction of Cr(VI) by reduction of potassium chromate, although it was unclear how these additions would affect weld soundness. A secondary gas mixture has been applied to interfere with the reaction between ozone and chromium to prevent CrO_3 formation (Ref. 10).

For situations where it is difficult to implement engineering controls, alternative

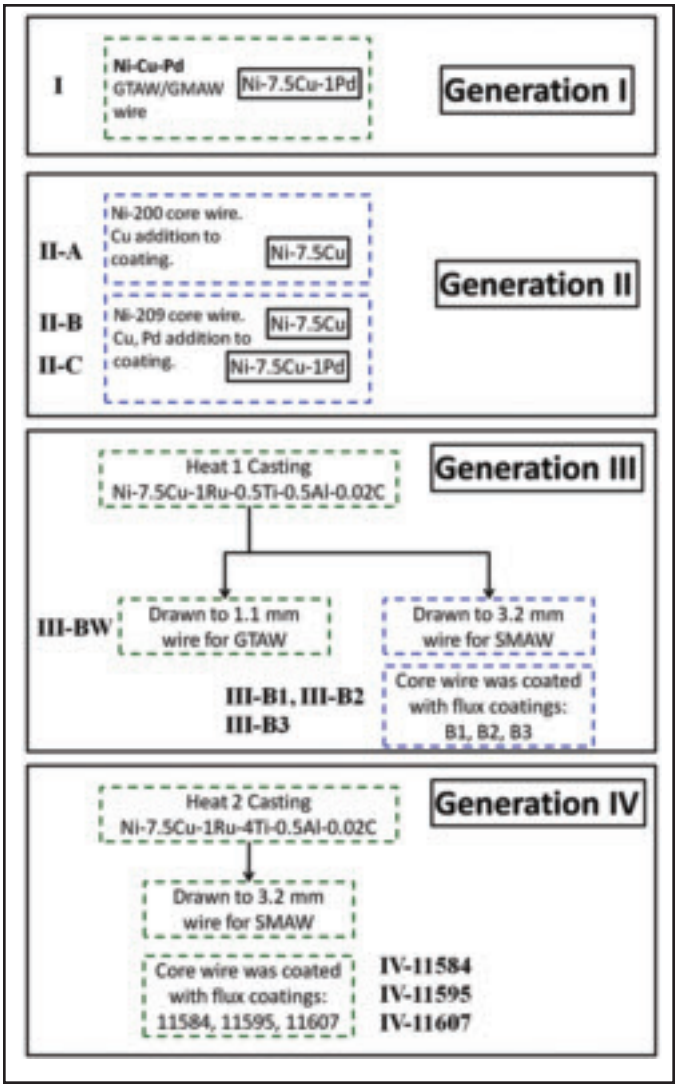

Fig. 1 — Ni-Cu welding consumable development chart showing nomenclature used to identify consumables for this study.

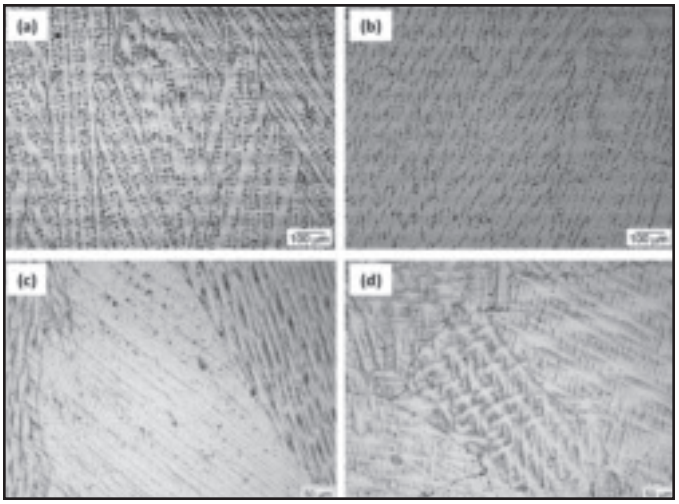

Fig. 2 — Representative weld metal microstructures of weld deposits. A — Generation II-B; B — II-C; C — III; D — IV.

approaches have been considered to minimize welder exposure to Cr(VI). One such approach was to investigate the possibility of using a filler metal that will produce satisfactory welds on stainless steel while minimizing the generation of Cr(VI) to acceptable limits in the welding fume (Refs. 11–15). Such a filler metal would need to have good weldability, corrosion characteristics comparable to common stainless steel alloys (such as Type 304), and ultimately lack the element Cr to prevent formation of Cr(VI) compounds during fume formation. Previous research showed that use of a welding consumable based on the Ni-Cu (Monel®) system to join stainless steel exhibited suitable corrosion resistance (Refs. 11–14), as well as weld compatibility and acceptable mechanical properties (Ref. 15).

The Ni-Cu system was selected based on its galvanic compatibility with austenitic stainless steel in chloride environments, and noble alloying elements such as Pd were added to increase resistance to localized corrosion phenomena such as pitting and crevice corrosion. The optimal composition to achieve adequate corrosion resistance was determined to be Ni-(5-10) Cu-1Pd (Ref. 12). Concentrations of Cr in the welding fume were reduced by a factor of 20 during welding of Type 304 stainless steel with Monel as a consumable (Ref. 15). Because the element Cr was not alloyed in the consumable, Cr present in the fume resulted only from vaporization of the base metal. The contribution to fume generation from the base metal has been shown to produce fume at a rate four orders of magnitude lower than the consumables themselves (Ref. 2); thus, Cr reductions in welding fume produced by a Cr-free consumable are expected to be significant.

Previous studies have focused primarily on testing the feasibility of using Ni-Cu consumables during welding of Type 304L austenitic stainless steel (Refs. 11–15). The studies utilized the gas metal arc welding (GMAW) and gas tungsten arc welding (GTAW) processes to deposit welds for evaluation of mechanical properties and corrosion resistance. Another target form of this welding consumable was for the shielded metal arc welding (SMAW) process because it is highly versatile, portable, and widely used. Also, stainless steel SMA welding generally has greater concentrations of Cr(VI) in the welding fume compared to bare wire processes (Refs. 2, 3). The current study reports on the development of a Ni-Cu-based consumable for the SMAW process as well as a bare wire consumable for the GTAW process. This study focused on evaluations of weldability throughout the development process to promote direct implementation of such a consumable. Weldability is defined by the American Welding Society as the capability of successfully fabricating a material by welding and the ability to have that material perform satisfactorily once placed into service (Ref. 16). Based on this definition, the following aspects of weldability were evaluated: mechanical behavior, corrosion resistance, weld cracking resistance, and fume generation rates and composition.

Consumable Development Summary

Welding consumables used in this study were developed in an iterative manner to achieve the optimum deposit composition and minimize potentially harmful fabrication-related issues (Ref. 17). Two types of welding consumables were used during experimentation: a bare wire electrode deposited with the GTAW process and several different SMAW consumables. These are defined using a "Generation" scheme based on the composition of the consumable. The generation classification is provided in Fig. 1, which includes the nominal composition and type of welding consumable. Directly outside of each box containing the different consumables of each generation are an abbreviation for each consumable type, for example II-A, II-B, and III. These abbreviation names are used for the remainder of the document. To meet corrosion require-

Table 1 — Generation II SMAW Consumable Compositions (wt-%) Determined with Mass Spectrometry and Interstitial Analysis

Consumables	C	Mn	Si	Fe	Cr	S	P	Cu	Ni	Al	Ti	Pd
Ni-209 core wire	0.021	0.24	0.21	—	—	—	—	—	94.5	0.046	4.29	—
Ni-Cu deposited weld metal	0.022	0.32	0.7	0.09	0.01	0.001	0.003	8.01	89.07	0.07	1.56	—
Ni-Cu-Pd deposited weld metal	0.016	0.147	1.08	0.08	0.04	0.005	0.005	4.94	bal	0.05	0.97	0.24

Table 2 — Compositions (wt-%) of Wire Drawn from Castings Used for Generation III and IV Wire Consumables as Determined with Mass Spectrometry and Interstitial Analysis

Consumables	C	N	O	S	P	Si	Cu	Ni	Al	Ti	Ru
Heat 1 (Generation III)	0.014	<0.001	0.0031	<0.001	<0.005	—	8.20	89.3	0.56	0.53	1.36
Heat 2 (Generation IV)	0.019	—	—	<0.002	<0.002	0.10	7.78	85.85	0.83	4.31	1.11

Table 3 — Compositions (wt-%) of Base Metals Used for Weld Deposits

Heat	Composition (wt-%)										
	C	Cu	Fe	Mn	Mo	Ni	Cr	Si	N	P	S
BM1 304L (6.4 mm)	0.03	—	bal	1.24	—	8.08	18.1	0.37	NA	NA	NA
9JA7 304L (6.4 mm)	0.02	—	bal	1.76	—	8.11	18.1	0.36	0.08	0.030	0.003
95L9 304L (9.5 mm)	0.01	0.41	bal	1.78	0.28	8.36	18.3	0.29	0.1	0.030	0.003

ments as shown below, target compositions of the consumables were Ni-7.5Cu-1Pd and Ni-7.5Cu-1Ru with other alloying additions to improve weldability.

The Generation I consumable was produced in limited quantity to evaluate the corrosion behavior and mechanical properties of the Ni-Cu-Pd target composition as reported elsewhere (Ref. 18). This consumable was used in conjunction with both the GTAW and GMAW processes to make high-quality welds.

Generation II consumables were the first SMAW consumables developed. Cu and Pd powders were added to a flux coating, which was extruded over Ni-200 and Ni-209 (Ni-209 provided better weld deoxidation than Ni-200) core wire. Compositions of the Ni-209 core wire, as well as Ni-Cu and Ni-Cu-Pd all-weld-metal deposits are shown in Table 1. All-weld-metal deposits were obtained by making a single weld pass with the SMAW consumables on a copper chill block.

Beginning with the Generation III consumables, additions of Cu and Ru were made directly to the core wire because transfer efficiency was determined to be insufficient to reach target levels in Generation II welds (see Table 1). The noble element Ru was found to be an acceptable alternative to Pd from a corrosion standpoint and at reduced cost (Ref. 19). A custom heat of filler metal material (target composition Ni-7.5Cu-1Ru-0.5Al-0.5Ti-0.02C) was cast with a two-stage vacuum induction melting and electroslag remelting (VIM/ESR) process to ensure alloy purity and homogeneity. The actual composition of the Ni-Cu-Ru casting (Heat 1) is provided in Table 2. The casting was extruded into 3.2-mm- (0.125-in.-) and 1.1-mm- (0.045-in.) -diameter wires for use with SMAW and GTAW, respectively. The SMAW wires were coated with three different batches of flux coatings. All of the coated consumables produced multipass welds that contained unacceptable levels of porosity. Surprisingly, single-pass welding was successfully performed, and it is surmised that some elements in the Type 304L base metal (probably Cr, Mn, and Si) aided in reducing porosity as they mixed with the molten weld pool during welding trials. Welds made with the bare wire GTAW process were free of porosity because argon shielding gas was used. In the current work, when Generation III welds are mentioned with regard to corrosion and weldability testing, they were deposited with the GTAW process (Generation III-BW) because the SMAW deposits contained significant levels of porosity in multipass welds. Gas tungsten arc welds contained the nominal composition that was desired of the SMA welds; therefore, much of the weldability evaluation utilized GTAW deposits. It should be noted that the GTAW wire has potential use with the GMAW process; however, such an evaluation was beyond the scope of the current study and further work would be required to evaluate GMA weldability.

A second heat of filler metal material (Generation IV) was produced containing increased Ti content (target composition of Ni-7.5Cu-1Ru-0.5Al-4Ti-0.02C). The actual heat composition is shown in Table 2. This ingot was reduced to 3.2-mm wire electrodes, which were coated with several iterations of flux coatings (designated 11584, 11595, and 11607) until satisfactory electrode operability was achieved as deemed by certified welders and staff who specialize in the development of flux-based consumables.

Experimental Procedures

Welding Procedures

Shielded metal arc welds were produced using 3.2-mm Generation II, III, and IV welding electrodes on 6.4- and 9.5-mm-thick Type 304L base metal (Table 3). Welding current was maintained in the range of 120–130 A, voltage between 24–25 V in the DC electrode positive configuration, and travel speed at approximately 2.5 mm s^{-1} for all welded samples produced with the SMAW consumables. During GTA welding with Generation III-

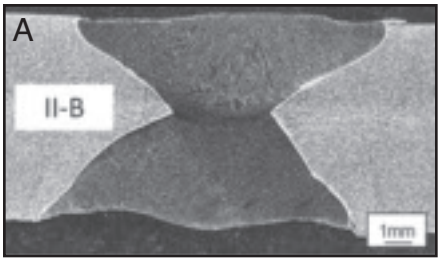

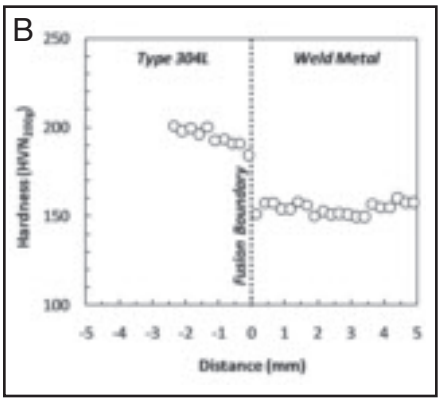

Fig. 3 — Representative across Generation II weld deposited on Type 304L stainless steel. A — Weld cross section; B — microhardness traverse.

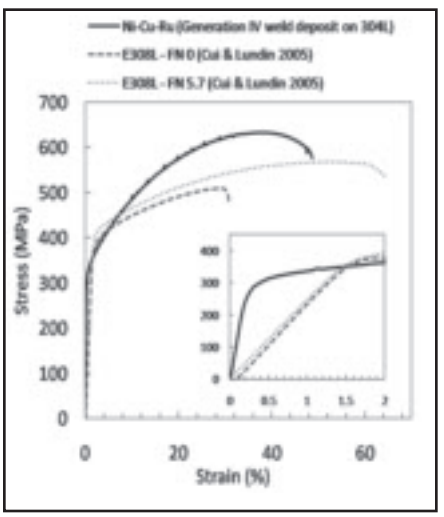

Fig. 4 — Stress-strain curve of Generation IV-11607 all-weld-metal deposit on Type 304L. Also included are stress-strain curves of E308L weld metal with (FN 0) and without (FN 5.7) microfissures for comparison (Ref. 29).

BW consumable, the weld deposits were made with a current of 200 A, voltage of 13.5 V, travel speed of 2.1 mm s^{-1}, and wire feed speed of 25.4 mm s^{-1} under 100% argon shielding gas. Gas tungsten arc welding was performed on a sidebeam carriage with automatic arc voltage control (set to 10% sensitivity) and a 300-A constant current power supply.

Mechanical Testing

Mechanical properties of welds were determined by tensile testing, guided bend testing, and Vickers microhardness tests.

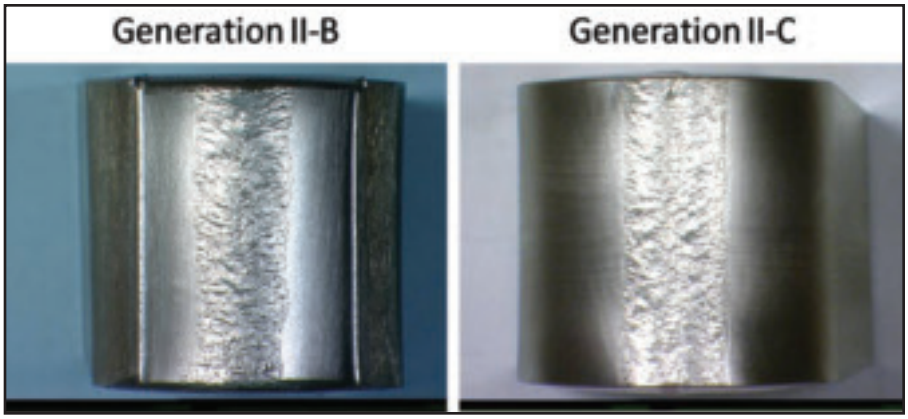

Fig. 5 — Bend test specimens that passed AWS guide bend testing requirements.

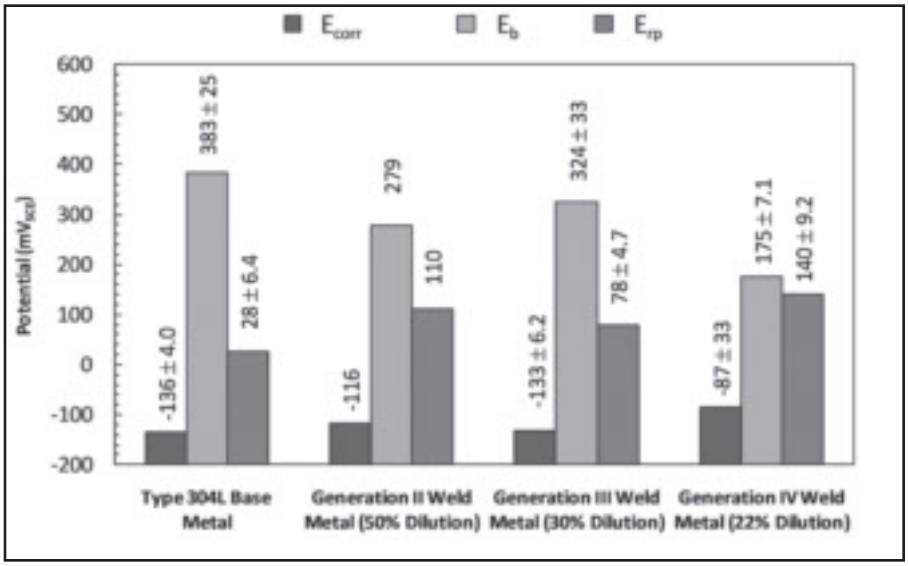

Fig. 6 — Summary of critical potentials of Generation II, III, and IV welds on Type 304L measured in 0.1 M NaCl solution. Corrosion potential (E_{corr}), breakdown potential (E_b), and repassivation potential (E_{rp}) are included.

Transverse weld tensile and bend specimens were tested according to the ANSI/AWS B4.0 standard (Ref. 20). Tensile testing was performed using a 500-kN servohydraulic load frame. Displacement rate was maintained at 0.085 mm s^{-1} during testing. Guided bend testing was performed on die blocks with either a 12.7- or 19.1-mm radius. Microhardness testing was performed with a diamond indenter at a load of 200 g and measurements were made on the Vickers scale.

Metallurgical Evaluation

Welds were sectioned for analysis with light optical microscopy (LOM) and scanning electron microscopy (SEM). Samples were mounted in conductive mount resin and then progressively ground with 240, 600, and 800 grit SiC paper. Final polishing was accomplished using 3 and 1 μm diamond suspension followed by a vibratory polish in 0.02-μm colloidal silica for 2 to 4 h. Etching was performed by swabbing with Marble's Reagent (10 g $CuSO_4$, 50 mL HCl, 50 mL distilled H_2O) for 2 to 10 s to achieve the desired effect. Light optical microscopy images were acquired with an inverted metallograph and digital camera. Scanning electron microscopy was performed at accelerating voltages of 10 to 30 kV. Semiquantitative chemical analyses were performed with energy-dispersive spectroscopy (EDS) using the ZAF correction method.

Corrosion Testing

Electrochemical corrosion tests were conducted on samples sectioned from GTA and SMA welds. Cyclic polarization tests were performed in aerated 0.1 M NaCl solution using a potentiostat set at a scan rate of 10 mV min^{-1}. A saturated calomel electrode (SCE) and a pure platinum mesh were used as reference and counter electrode, respectively. Air was

Table 4 — Mechanical Properties of Weld Deposits on Type 304L Stainless Steel

Material Type	0.2% Proof Stress (MPa)	Tensile Strength (MPa)	Elongation (%)	Reduction in Area (%)	Failure Location
304L Minimum	170	480	40	50	—
II-B	—	597	—	—	Weld metal
II-C	—	531	—	—	Weld metal
III-BW	279*	540	52*	54*	Weld metal
IV-11607	295*	618	48*	44*	Weld metal
E308L-XX	—	520 min	35 min	—	—

*Values obtained from all-weld-metal tensile tests.

Table 5 — Summary of Guide Bend Test Results of Generation II, III, and IV Weld Deposits

Consumable	Sample	Radius (mm)	Approximate Outer Ligament Strain (%)	Comments
II-B	1	19	13	Few small microcracks*
	2	19	13	No microcracks*
	3	12.7	18	No microcracks*
	4	12.7	18	No microcracks*
II-C	1	12.7	18	Crack originating from weld defects
	2	12.7	18	Crack originating from weld defects
	3	12.7	18	No microcracks*
	4	12.7	18	No microcracks*
III-BW	1	12.7	18	No microcracks*
	2	12.7	18	<10 microcracks
	3	12.7	18	No microcracks*
	4	12.7	18	1 microcrack*
IV-11607	1	12.7	18	1 microcrack*
	2	12.7	18	<10 microcracks
	3	19	13	No microcracks*
	4	19	13	No microcracks*

*Passes the requirements of AWS D1.6:1999/4.6.5.

bubbled through the solution for aeration. Prior to initiating scans, the sample open circuit potential was allowed to stabilize for a period of 1–2 h.

Slow strain rate testing (SSRT) was employed to assess the susceptibility of the samples to stress corrosion cracking (SCC). Tensile specimens were made according to ASTM standard E8 (Ref. 21). For welded samples, the tensile specimens were fabricated transverse to the weld with the weld in the center of the gauge section. The surface of the tensile bar was polished to 1 μm to prevent microcracks. Specimens were tested at a strain rate of 3×10^{-7} s^{-1} both in air and in 25 wt-% NaCl solution at pH 1.5. After experiments, fracture surfaces were examined by SEM. All SSRT experiments were performed at ambient temperature.

Weldability Testing

Gleeble®-based weldability testing was performed on transverse weld deposits to determine weld metal liquation cracking and ductility dip cracking (DDC) susceptibility using the hot ductility and strain-to-fracture (STF) tests, respectively. Hot ductility testing was performed using a sample free span of 25.4 mm and heating rate of 111°C s^{-1} (200°F s^{-1}). On-cooling hot ductility tests were free cooled at a rate of approximately 30°C s^{-1} (54°F s^{-1}). Samples were tested in tension at a stroke rate of 50.8 mm s^{-1} at the desired test temperature for both on-heating and on-cooling tests. Area reduction was used as an indication of ductility and was calculated based on measurements of initial and final cross section using calibrated precision calipers. Strain-to-fracture testing was performed by making an autogenous spot weld at the center of a dogbone specimen with weld metal deposited at the reduced cross section. The specimens were heated to the desired test temperature and strained. Cracking was evaluated in the spot weld as a measure of DDC susceptibility. Detailed STF testing procedures used in the current study are reported elsewhere (Ref. 22).

Transvarestraint testing was performed on weld deposits made on Type 304L base metal with Generation II and III-BW consumables to evaluate solidification cracking susceptibility. Deposits were machined flat and cleaned with acetone prior to performing the Varestraint test. Welding parameters were set to 180 A, 10 V (~2 mm arc length), at a travel speed of 2.1 mm s^{-1}. The total weld length was 50.4 mm, and the welds were strained at a length of 38.1 mm and ram speed of 152.4 mm s^{-1}. The amount of augmented strain imparted into the samples was controlled by changing die blocks where an increase in strain was accomplished with smaller die block radii. Type C thermocouples were plunged along weld centerlines at the back of the weld pool to acquire time-temperature history on-cooling after the bending portion of testing. Time-temperature data were recorded with a data acquisition system at 4 kHz acquisition rate.

Fume Analysis

Fume generation rates (FGR) were measured using a bulk fume collection hood that was modified from an American

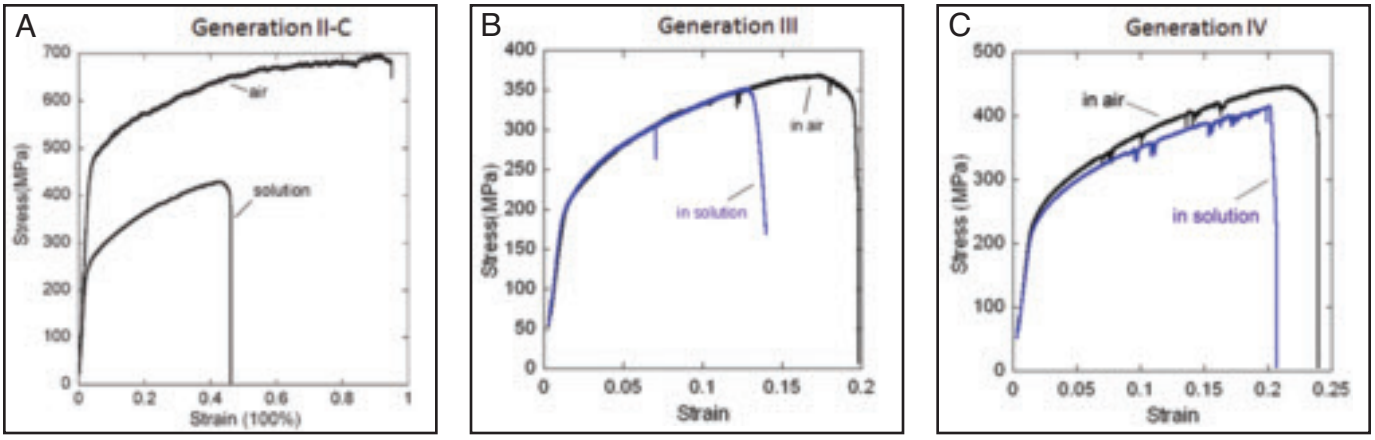

Fig. 7 — Slow strain rate testing curves for welds in air and 25 wt-% NaCl solution at pH 1.5 at strain rate of 3×10^{-7} s^{-1}. A — Generation II; B — Generation III; C — Generation IV. Note different scales on horizontal and vertical axes.

Welding Society standard (Ref. 23). The modified system employed glass fiber (HEPA-type) filters during collection, which have more than 99.9% collection efficiency of fume particle sizes greater than 0.3 μm. Filters containing the collected fume were subject to phase identification with X-ray diffraction (XRD) and wet chemical analysis for determination of Cr(VI) concentration. Fume collection was performed in accordance to a procedure described in detail elsewhere (Ref. 24). Fume was collected on 0.3-μm glass fiber filters that were weighed before and after collection. Fume generation rates were determined by the mass increase on the filter divided by the welding time. Filters were subject to XRD using step size of 0.03 deg (2θ deg) and dwell time of 22 to 25 s per step. Samples were submitted to an ISO certified testing lab for determination of Cr(VI) with standardized visible absorption spectrophotometric techniques. The Cr(VI) content was reported by the testing lab to an accuracy of 0.001 wt-%.

Results and Discussion

Weld Microstructure

Microstructural observation of deposited weld metal made with Generation II, III-BW, and IV consumables on Type 304L revealed a primary austenite (gamma fcc) solidification structure with indications of secondary phases along solidification grain (SGB) and subgrain boundaries (SSGB). Secondary phases were extracted from the matrix of various weld deposits by electrolytic dissolution of weld metal in a 10% HCl-methanol solution. Solutions were filtered through 0.2-μm pore size filters to collect the extract. X-ray diffraction analysis of the secondary phase extract identified particles as titanium-carbonitrides, i.e., Ti(C,N). Regardless of the amount of dilution by Type 304L, all welds were fully austenitic as is consistent with predictions from weld constitution diagrams such as the Schaeffler Diagram (Ref. 25). The weld metal exhibited a columnar grain structure characteristic of austenitic welds observed in fully austenitic Ni-based and stainless steel weld deposits (Ref. 26). Single-pass welds exhibited epitaxial nucleation from the Type 304L base metal, and multipass welds exhibited epitaxial nucleation from prior weld deposits. A primarily cellular or cellular-dendritic substructure was observed within the columnar grains. The primary cell or dendrite arm spacing was on the order of 20 μm regardless of the welding consumable or heat input. Representative weld metal microstructures are shown in Fig. 2A–D for Generations II-B, II-C, III-BW, and IV, respectively.

Migrated grain boundaries (MGB) were observed in the microstructure of all weld deposits. The grain boundary migration behavior of Generation III-BW and IV-11607 deposits varied significantly, even though weld target compositions were nominally the same. The MGBs in the Generation IV deposits were much more tortuous in nature than those observed in the Generation III deposits. Qualitative metallographic estimates revealed a higher volume fraction of precipitates in the Generation IV weld microstructure, which resulted in more grain boundary pinning and a higher degree of tortuosity than observed in the Generation II weld microstructure. The observed differences in precipitate distribution were primarily due to variations in Ti and C concentrations in the two types of weld deposits. Generation III-BW weld metals contained only 0.5 wt-% Ti whereas the Generation IV wires contained approximately 1 wt-% Ti. (Note that the core wire contained 4 wt-% Ti, but much of this was lost in the arc.) The Generation IV fluxes contained approximately 12% $CaCO_3$ whereas the Generation III-BW welds were produced under inert Ar gas during GTA welding. Carbonates are typically used to create a protective atmosphere over the weld pool and to facilitate arc stability and welding electrode operability (Ref. 27), and can result in an increase in C concentration in weld deposits. Higher C and Ti concentrations present in the Generation IV-11607 deposits result in a higher fraction of carbides in the weld metal of this consumable. The formation of these carbides appeared to have an effect on the solidification substructure, which exhibited more branching of secondary dendrite arms. The boundary pinning effect on the IV-11607 weld metal migrated grain boundaries was also observed to be much greater in comparison to the III-BW deposits. This is caused by the increased Ti(C,N) content (Ref. 28) and the more tortuous nature of SGB intersections associated with the cellular dendritic structure (Ref. 29). The effect of Ti(C,N) on solidification and solid-state cracking is discussed below.

Mechanical Properties

Vickers microhardness traverses typically exhibited lower hardness levels in the weld metal relative to the Type 304L base metal and heat-affected zone (HAZ). Figure 3A shows a double V-groove weld made with the Generation II consumable on Type 304L base metal, and B is a microhardness traverse (250 μm indent spacing) taken across the cross section. Note that Vickers hardness number (VHN) values in the base metal were approximately 200 VHN while weld hardness values were on the order of 150 to 160 VHN for all generations of weld deposits.

Tensile testing was performed transverse to the weld according to ANSI/AWS B4.0-98 standard to evaluate mechanical performance of welds produced with the Ni-Cu consumables on Type 304L base material. Results of tensile testing are

summarized in Table 4 where each value is an average of four tests. Ultimate tensile strength of Generation II, III-BW, and IV weld deposits exceeded the minimum required values of Type 304L. All deposits exceeded the minimum strength values required for E308-XX SMAW deposits, where XX stands for 15, 16, and 17. Mechanical property values of Type 304L (hot finished and annealed) and E308-XX class consumables (all-weld-metal deposits) are from handbook (Ref. 31) and standard sources (Ref. 32), respectively. Generation II-B and IV-11607 weld deposits had the highest measured strength levels whereas Generation II-C deposits had the lowest mechanical performance based on tensile strength. Some of the welds deposited with this electrode contained incomplete fusion defects and a higher degree of slag inclusions based on radiographs. This is believed to be the cause of the lower mechanical performance. The III-BW had lower tensile strength values than Generation II and IV deposits. This was due to the fact that welds were made with the GTAW process, which typically lacked the inclusions (and had a lower volume fraction of precipitates) that could have promoted strengthening and decreased ductility. All transverse tensile test failures occurred in the weld metal, indicating that the tensile strength of the Type 304L base metal was well above the required minimum.

Additional tensile specimens were made so that all-weld-metal properties could be determined. This was accomplished by depositing multiple weld passes in a groove (~19 mm wide × 3.3 mm deep) machined into Type 304L plate. The Type 304L backing was machined away after filling the groove with weld metal, resulting in a reduced section containing all weld metal. A 12.7-mm extensometer was used during tensile testing of the Generation III-BW and IV-11607 weld deposits, thus the extensometer was entirely within the width (~19 mm) of the multipass transverse weld deposit. In using an extensometer gauge length that was narrower than the weld deposit, erroneous measurements induced by nonhomogenous dissimilar weld mechanical properties were avoided. Although these are not the standard all-weld-metal tensile tests, this method provided a good estimate of weld metal properties (including proof stress, elongation, and area reduction) in the transverse direction. A typical stress-strain curve obtained with this procedure is shown in Fig. 4, which was measured for a Generation IV-11607 all-weld-metal deposit. Note that the inset in the figure is an enlarged portion of the elastic region of the curve. Also included on the plot are stress-strain curves for two E308-type consumables with different ferrite numbers (FN) – FN 5.7 and FN 0 (Ref. 30). The weld with FN 0 contained some small cracks whose nature was not identified. In the past, these have been termed "microfissures" (Ref. 30), but this term has no meaning with respect to the cracking mechanism. This test method showed that Generation III-BW and IV-11607 deposits exceeded minimum elongation requirements of E308-XX SMAW deposits. It is evident from the reported values of mechanical properties that Ni-Cu consumables are able to meet the minimum mechanical performance requirements of current Type 308 stainless steel consumables based on the AWS design code for filler metals.

Table 6 — Calculated SCTR and DDC-TR Values for Generation II and III Weld Deposits. Other Nickel-Based Alloys and Stainless Steels Are Included for Comparison (Ref. 34)

Material	Dilution Level by Type 304L	SCTR (°C)	DDC-TR (°C)
Generation II-B	~14%	111 ± 7	855–1055
Generation II-C	~10%	109 ± 6	770–1140
Generation III-BW	~11%	113	920–1130
Type 304L (FN6)	—	31	—
Alloy 617	—	85	—
Type 310 SS	—	140	—
Alloy 625	—	210	—

Table 7 — Summary of Important Hot Ductility Parameters of Generation II-C and III Deposits on 304L. Data Are Reported in °C

Hot Ductility Parameter	Generation II-C (~40% dilution)	Generation III-BW (~20% dilution)
NDT	1300	1360
NST	1333	1374
DRT	1300	1320
CSR (NST-DRT)	33	54
DDC-TR	850–1150	800–1100

Guided bend tests were performed on samples made from Generation II-B, II-C, III-BW, and IV-11607 weld deposits on 304L. Results of the bend tests are summarized in Table 5. The four II-B welds passed the requirements of AWS D1.6:1999, *Structural Welding Code — Stainless Steel*. Two of the II-C samples passed these requirements and two cracked due to preexisting, incomplete fusion defects associated with sample fabrication. Bend testing of III-BW deposits showed microcracks in two of the tested weld deposits though there were no macroscopic failures. Three of the four samples passed AWS standard minimum requirements. The Generation IV weld deposits were tested over two bend radii, 12.7 mm (0.50 in.) and 19 mm (0.75 in.). Samples passed the code requirements at the lower elongation values, which conforms to AWS consumable qualification standard minimums for Ni-based alloys (19-mm die block). Representative bend test samples that passed the requirements of AWS D1.6 are shown in Fig. 5.

Corrosion Evaluation

Corrosion compatibility of the Ni-Cu consumables with austenitic stainless steel was a requirement from the start of this work because stainless steels are used in corrosive environments (Refs. 11, 12, 14). The results of initial work showed corrosion compatibility in chloride-containing environments of dissimilar welds consisting of a Ni-Cu-based welding consumable containing the noble element palladium and austenitic stainless steel. Further work showed that a GTA and SMA consumable based on the Ni-Cu-Pd system were also compatible for stainless welding (Ref. 18). The use of ruthenium was investigated as an alternative to Pd because the cost of platinum group metals fluctuate with time, and Ru is typically the least expensive of the platinum group metals. This compatibility was obtained based on the following corrosion design criteria (Ref. 11): 1) the breakdown potential and repassivation potential of the weld metal were required to be greater than the corrosion potential of the stainless steel base metal to avoid localized corrosion such as pitting or crevice corrosion; and 2) the corrosion potential of the weld metal was required to be equal to or greater than the corrosion potential of the stainless steel to cathodically protect the weld.

Based on electrochemical corrosion testing of Generation II, III-BW, and IV weld deposits on Type 304L, the corrosion design requirements were satisfied. A summary of the critical electrochemical potentials is shown in Fig. 6 where measured potentials are plotted for each generation of consumable in comparison to Type 304L. Potentials were measured vs. a saturated calomel electrode (SCE). Aver-

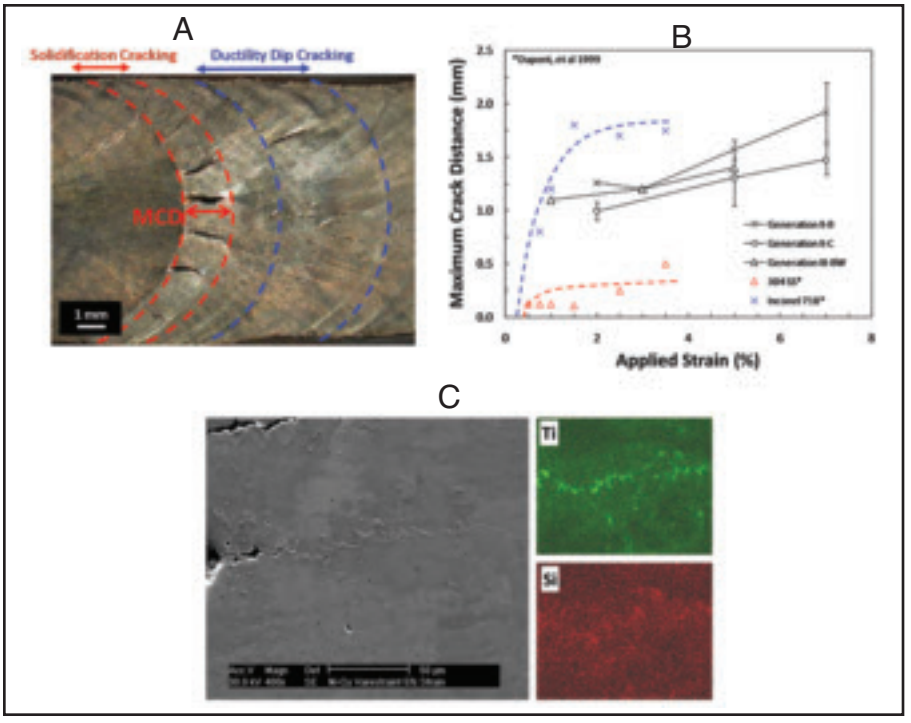

Fig. 8 — Analysis of the following: A — Cracking regions associated with Generation II deposit; B — solidification cracking envelope of Generation II and III weld deposits, including data of 304L and Alloy 718 (Ref. 35); C — composition map of solidification crack in Generation II-B weld deposit.

age values were calculated from at least three experimental runs, and standard deviations are indicated for Generations III and IV of those runs. The breakdown (E_b) and repassivation (E_{rp}) potentials of the Generation II, III, and IV welds on Type 304L were greater than the corrosion potential (E_{corr}) of Type 304L, thus satisfying the first corrosion design requirement. Also, the corrosion potential of the Generation II (–116 mV_{SCE}), III (–133 mV_{SCE}), and IV (–87 mV_{SCE}) weld metals were greater than the corrosion potential of Type 304L (–136 mV_{SCE}), satisfying the second design requirement. Differences in corrosion potentials between the various generations of weld deposits may be attributed to slight variations in consumable composition and the extent of weld dilution. The higher volume fraction of secondary phase particles in the Generation II and IV deposits may also have resulted in increased pitting susceptibility with respect to Generation III deposits, hence the lower breakdown potentials (Ref. 33). However, even with large variations of weld dilution levels, weld deposits met the design criteria. This suggests that these consumables would be considerably tolerant to variations in dilution from a corrosion perspective.

Slow strain rate testing (SSRT) was performed to assess the stress corrosion cracking (SCC) susceptibility of welds in a chloride-containing environment. Slow strain rate testing specimens were machined from welds deposited with Generations II, III, and IV consumables. These samples were tested in 25 wt-% NaCl solution (pH 1.5) at a strain rate of 3×10^{-7} s^{-1} and at ambient temperature. Results of tests conducted in air and in the solution are shown in Fig. 7A–C. As the figure shows, ductility was higher in air than in the NaCl environment for all three generations of weld deposits. The observed disparity between air and solution was most pronounced in Generation II welds. Examination of fracture surfaces of the Generation II welds tested in solution revealed that failure occurred in the weld metal and was associated with brittle transgranular features. Generation III-BW welds had lower ductility than Generation II, which may be attributed to some welding defects that occurred during sample fabrication (such as incomplete fusion). However, comparing the Generation III SSRT in air to that in solution still shows reduction in strength and ductility suggesting some susceptibility to SCC. Generation IV weld deposits also showed some reduction in strength and ductility, although the observed difference was not as great as that seen in Generation III welds. Most of the fracture surface of Generation III and IV SSRT samples was in the Type 304L HAZ adjacent to the fusion boundary. Fe-Ni-Cr alloys containing high concentrations of Ni generally have good resistance to SCC according to the well-known Copson curve (Ref. 34), and all of the weld deposits in the current study contained high concentrations of Ni. Based on the Copson curve, one would expect the weld deposits to have significantly longer failure times than Type 304L base material used, which have the shortest failure times on the curve. Because the fabricated samples were not all weld metal, it is probable that the SCC susceptibility of the stainless steel HAZ is dominating the sample failure behavior during the testing. This concept is supported by the observation that fractures of Generation II and III deposits occurred mostly in the stainless steel (Refs. 18, 19).

Weldability Evaluation

During fabrication, Ni-based alloys can be susceptible to solidification and liquation cracking, as well as the solid-state cracking phenomenon known as ductility dip cracking (DDC) (Ref. 26). Therefore, three different weldability tests were performed to assess susceptibility to high-temperature weld cracking. The Varestraint test was used to evaluate weld solidification cracking susceptibility. The hot ductility test was used to evaluate propensity to weld metal liquation cracking and to assess overall weld metal ductility. The strain-to-fracture test was used to evaluate susceptibility to DDC. Results of these tests are presented and discussed below.

Solidification Cracking

Based on previous transvarestraint testing results, Ni-based alloys have been shown to have a higher solidification cracking susceptibility than Type 304L/308L stainless steels (Refs. 35, 36). These stainless steels solidify under the ferrite-austenite (FA) mode, where primary ferrite solidification is followed by a peritectic-eutectic transformation to austenite (Ref. 37). Weld metal that solidifies under the FA mode generally has high resistance to cracking due to the tortuous nature of SGB intersections, which prevents continuous wetting of liquid films along grain boundaries, and the generally poor wetting of liquid films along ferrite-austenite boundaries. Fully austenitic solidification results in welds with lower inherent resistance to solidification cracking because SGB intersections tend to be straight and susceptible to liquid film wetting. The austenite phase also has a greater tendency to promote segregation of solute elements to grain boundaries than ferrite due to lower inherent solubility of solute elements. For example, the impurity elements S and P have lower solubility in austenite resulting in higher concentrations along grain boundaries as a result of solidification-induced segregation (Ref. 38). Therefore, solidification cracking is of concern when switching from a stainless steel consumable to a Ni-based welding consumable. Consequently, the

Table 8 — Fume Generation Rates of Generation II and IV SMAW Consumables

Consumable	Current (A)	Arc voltage (V)	Arc Power (kW)	Weld Heat Input (kJ/mm)	Average Fume Generation Rate (g/min)	Standard Deviation	Cr(VI) Content in Bulk Welding Fume (wt-%)
E308-16 low HI	80	24.0	1.92		0.09		2.60
E308-16 high HI	115	28.3	3.25	0.68	0.20	0.031	
Generation II-B	115	28.5	3.27	0.73	0.55	0.027	
Generation II-C	110	25.5	2.81	0.61	0.41	0.003	0.020
Generation IV-11607 low HI	90	22.5	2.03	1.1	0.41	0.042	0.057
Generation IV-11607 high HI	120	24.5	2.94	1.4	0.58	0.025	0.097

cracking susceptibility of Ni-Cu-based welds deposited on Type 304L was investigated using the transvarestraint test.

Generation II-B, II-C, and III-BW deposits were made by filling machined grooves in stainless steel to achieve dilutions of approximately 14, 10, and 11%, respectively. The deposits were subjected to at least three strain levels during transvarestraint testing to develop a cracking envelope. Maximum crack distances (MCD) were measured on each tested coupon. Solid-state cracks were observed and counted as well, and the results of the observations are reported in Table 6. Note that only one test was performed at each strain condition for the Generation III-BW deposit due to limited availability of filler metal, so statistical analysis was not performed for those measurements.

Two distinct regions of cracking were observed in all three types of weld deposits. The first range was directly behind the instantaneous liquid-solid interface at the moment strain was applied. This region was associated with weld solidification cracking because it was within the solidification temperature range. The second region where cracking was observed was remote to the solidification cracks, and it was typically observed several millimeters behind the weld region where grain boundary liquid films were not present. Therefore, the second region of cracking occurred in the solid state and is indicative of DDC. Both regions of cracking are shown in the Generation II-B Varestraint test weld depicted in Fig. 8A. The particular sample shown was tested at 7% strain. Note that because a root opening of more than 1 mm exists between the two regions of cracking, the mechanism for cracking is clearly different and associated with a different temperature range.

Maximum crack distances were plotted as a function of applied strain, as shown in Fig. 8B, for each of the three weld deposits. For comparative purposes, the maximum crack length (MCL) of Type 304 and Alloy 718 transvarestraint tests were included on the plot (Ref. 36). Type 304 has a low susceptibility to solidification cracking whereas Alloy 718 has a moderate to high solidification cracking susceptibility. The MCD values of Ni-Cu welds deposited on 304L fall between those of the other two alloys. Although MCD and MCL are not equivalent (MCD is usually slightly less than MCL), the values are usually sufficiently close to allow comparison of solidification cracking behavior. Based on this assumption, the Ni-Cu consumables appear to have a moderate susceptibility to solidification cracking, according to measured crack distances at strain levels between 1 and 7%.

Note that threshold cracking strains were not measured as shown for the Alloy 718 and Type 304 alloys. Threshold strain is the minimum strain to cause solidification cracking and appears to be less than 0.5% for 718 and 304. The II-B deposits appeared to have the highest cracking susceptibility of the three types Ni-Cu weld deposits. The II-C and III-BW deposits appeared to have similar cracking susceptibility but based on the error bars of the II-C deposit, and the lack of replications of the III-BW deposit, this similarity may not be statistically significant.

Analysis with SEM and EDS composition mapping revealed that solidification cracks were associated with liquid films rich in Ti and possibly Si, as shown in Fig. 8C. The figure shows the leading edge of a solidification crack of a Generation II-B deposit. This deposit had the highest Ti concentration of the three deposits and also the highest cracking susceptibility. The dense distribution of Ti(C,N) particles was a result of a eutectic reaction at the end of solidification. Such a reaction would effectively promote solidification cracking because a continuous liquid film develops along the solidification grain boundaries (Ref. 26). These liquid films provide little accommodation for any augmented strain (or solidification-induced shrinkage strain during welding), which results in cracking. This indicates why the II-B deposit exhibited the highest susceptibility.

The susceptibility to solidification cracking was further quantified by calculating the solidification cracking temperature range (SCTR). Saturated strain levels are determined by plotting MCD as a function of applied strain. When MCD reaches a value where it does not increase with further increases in strain, it has reached the saturated value. This represents the maximum length along the weld where susceptible microstructure exists. That is to say, cracking extends over the entire length of a grain boundary where a continuous liquid film is present along a grain boundary, assuming there is no crack propagation in the solid state (i.e., DDC). Based on the cracking envelope shown in Fig. 8B, the saturated MCD might not have been reached because values of MCD appear to be increasing even up to 7% strain. Therefore, the MCD at the highest applied strains for each material was used for calculating SCTR values with the following equation:

$$SCTR = CR\frac{MCD}{V}$$

where the cooling rate (CR) was measured with a thermocouple in the solidification temperature range (~170° to 200°C s^{-1}), and V was the torch travel speed (2.1 mm s^{-1}) during the test.

Calculations of SCTR values at maximum strain are presented in Table 6 for the Generation II and III-BW weld deposits. Several other stainless steels and Ni-based alloys are included for comparison (Ref. 35). The SCTR assessment shows a similar trend as seen in the cracking envelope in Fig. 8. The Type 304L stainless steel has the lowest SCTR value (31°C) and hence the lowest propensity for solidification cracking. Generation II and III-BW weld deposits have SCTR values of approximately 110°C indicating a higher susceptibility to cracking than Type 304L, although similar in value to other Ni-based alloys such as Alloy 617.

Temperatures over which DDC occurred were estimated using a similar ap-

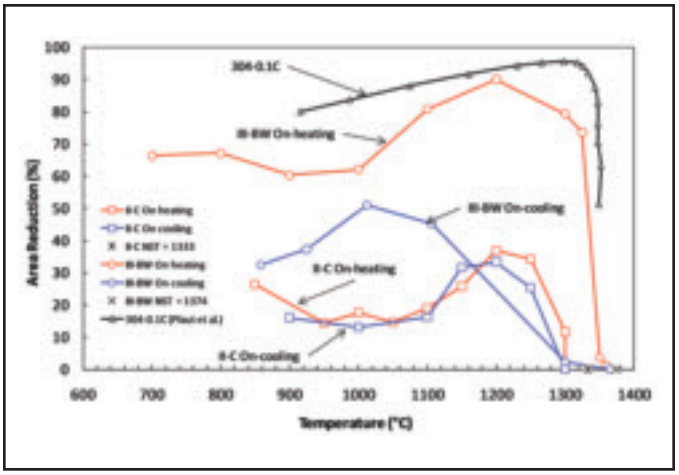

Fig. 9 — Hot ductility curves of Generation II-C and III-BW welds deposited on Type 304L and wrought Type 304 from (Ref. 40).

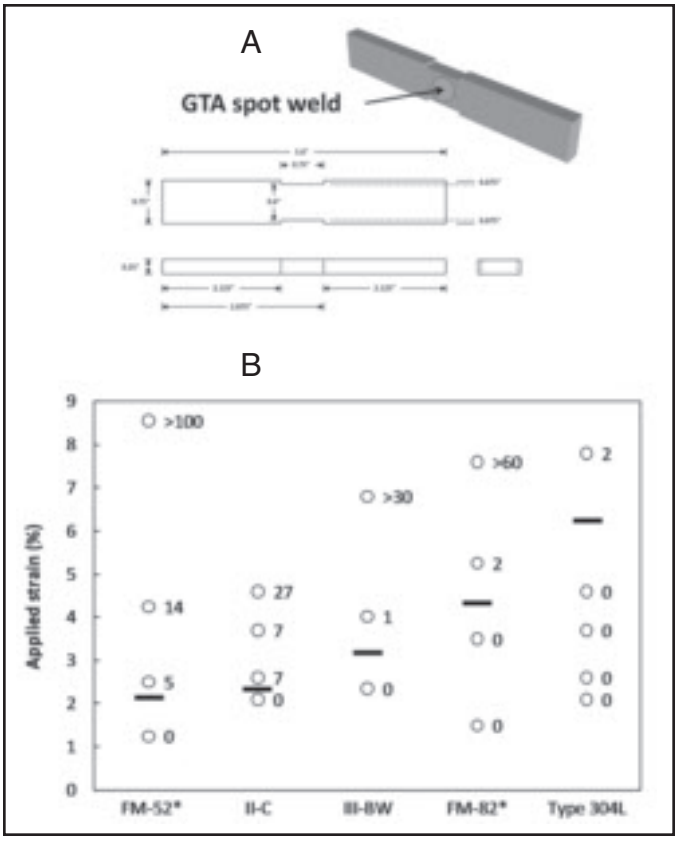

Fig. 10 — A — Strain-to-fracture test sample schematic; B — test results of Generation II and III welds compared to other Ni-based filler metals (Ref. 42) and Type 304L tested at 950°C. The number of cracks observed on each specimen is listed.

proach to the SCTR calculation. Ductility dip cracking occurred in multiple locations and orientations relative to travel direction and had a variety of lengths between fractions of a millimeter to several millimeters in length. The upper and lower temperatures of the cracks were calculated by including the entire range where cracks were observed. The calculated ranges are also included in Table 6, which shows the lower and upper temperature limits. These temperature ranges are discussed below.

All of the weld deposits analyzed during the present work solidified as austenite. Austenite solidification is promoted by the high Ni-equivalent values of the weld deposit. Therefore, it is suggested that impurities be minimized when welding stainless steels with Ni-Cu consumables because they will easily wet austenite grain boundaries. This is generally achieved by proper handling of welding consumables and base metals to ensure cleanliness. Weld zones must be kept cleaner to avoid entrapment of oxides and embrittling elements such as S, P, and Pb (Refs. 39, 40). Weld procedures should call for low P + S grades of base material to ensure weld deposits do not pick up impurities from the base metal. However, impurity pickup may be an issue during weld repair of older heats of stainless steel that may have been put into service before impurity refining became tightly controlled. An upper limit of approximately 0.01 wt-% P + S is necessary to avoid solidification cracking in stainless steel weld deposits with high Ni equivalency, i.e., fully austenitic (Ref. 41). Such values would likely be an acceptable upper limit for impurity control during welding of vintage stainless alloys with the Ni-Cu consumables developed here. It was also evident that segregation of Ti and Si contribute to solidification cracking suggesting that levels of these elements should be controlled to values within those of the current weld deposits. Weld dilution plays a critical role on solidification cracking susceptibility as demonstrated in a study of Monel welding on Type 304L, which showed cracking could be avoided if dilution was less than 30% (Ref. 12). Another study of the Fe-Ni-Cu ternary system showed that solidification cracking was exacerbated as Cu contents were increased above approximately 10–15 wt-% over a broad range of Ni-Fe concentrations in GTA welds (Ref. 42). While these two studies considered higher Cu concentrations than the current study, they both suggest that controlling dilution is a critical factor in maintaining solidification cracking resistance. Therefore, as general practice, it is recommended that dilution for the current consumables be limited to approximately 30%.

Weld Metal Hot Ductility

The hot ductility test has been widely used (Ref. 26) to evaluate the weldability of Ni-based alloys and stainless steels because elevated-temperature cracking can usually be directly associated with a loss in available ductility. Using the hot ductility test, on-heating and on-cooling curves were produced for transverse multipass weld deposits of Generation II and III consumables on Type 304L. The dilution levels (by Type 304L) of the weld deposits were approximately 40% and 28% for the Generation II-C and III-BW deposits, respectively. Hot ductility curves for both weld deposits are shown in Fig. 9 and a summary of measured hot ductility behavior is listed in Table 7.

On-heating curves for both deposits increased in ductility up to peak temperatures of approximately 1200°C. Ductility decreased as test temperatures were increased above this temperature and reached zero ductility above 1300°C. The temperature of zero ductility on-heating corresponds to the nil-ductility temperature (NDT). The NDT is the temperature where the weld metal grain boundaries were coated with continuous liquid films resulting in a complete loss of ductility although the films still maintain some load-carrying capacity. Nil-ductility temperature values of the Generation III deposit was approximately 1360°C, a value considerably higher than that observed in the II-C deposit.

An additional test was performed on-heating called the nil-strength temperature (NST) test. Approximately 25 kg of tensile load was placed on the test samples, and they were heated until failure. The value for NST represented the temperature at which sufficient grain boundary liquid was present to allow failure at very low loads. Nil-strength temperature values were found to be 1333° and 1374°C for the Generation II-C and III weld deposits, respectively. The LOM and SEM

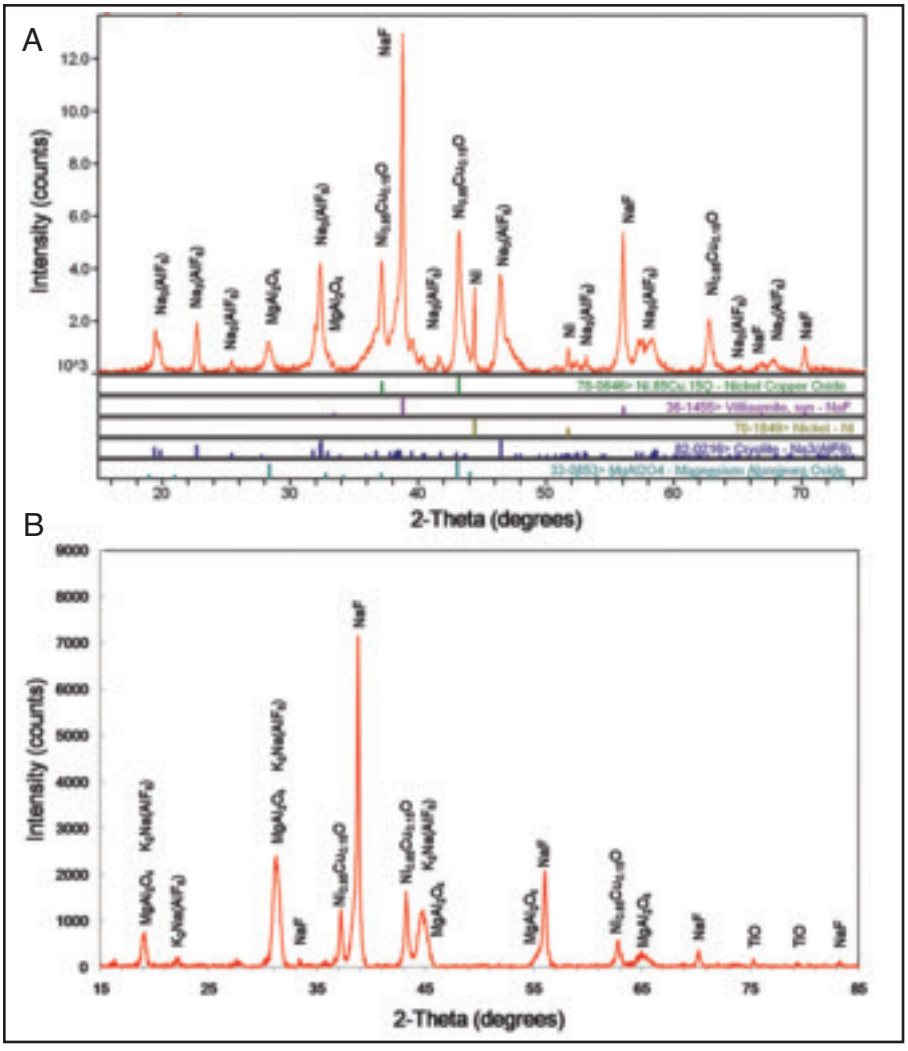

Fig. 11 — X-ray diffraction spectra of welding fume produced by SMAW consumables during welding of Type 304L. A — Generation II; B — Generation IV.

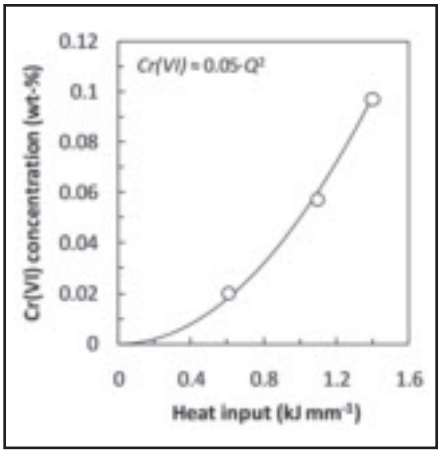

Fig. 12 — Concentration of Cr(VI) in welding fume as a function of heat input.

evaluation of the NST fracture specimens revealed that cracking occurred extensively along SGB and SSGB locations and that fractures were dendritic in nature. EDS of the fractures indicated that the liquid films coating the dendrite regions were rich in Ti and Si. This suggests that the eutectic containing Ti(C,N) particles in lower freezing point interdendritic regions undergo liquation.

On-cooling hot ductility tests were performed by heating test samples to a temperature midway between NDT and NST (II-B samples were heated to 1315°C and III-BW samples were heated to 1365°C), then cooling to a predetermined temperature before pulling the sample to failure. The temperature at which the alloy recovers some ductility (~5%) on-cooling is termed the ductility recovery temperature (DRT). These DRT values were determined to be approximately 1300° and 1320°C for the II-C and III-BW weld deposits, respectively. Ductility of both deposits appeared to recover at similar rates upon decreasing temperature from the DRT, although the Generation III deposit recovered more overall ductility upon cooling, which implies that it has a higher resistance to solid-state cracking below approximately 1150°C.

The difference between the NST and DRT is considered the crack-susceptible region (CSR = NST – DRT). Ductility in a multipass weld HAZ is essentially zero within this temperature range due to the presence of liquated grain boundaries. If a weldment experiences prolonged duration in this region, stress will accumulate during cooling of the weld increasing the likelihood of cracking (Ref. 43). The Generation II-C weld deposits had a CSR of approximately 33°C, which represents the temperature range in which the weld metal may be susceptible to cracking phenomena such as weld metal liquation cracking in the HAZ of a multipass weld. The Generation III deposit had a CSR of approximately 54°C, which was larger than the CSR of II-C welds. However, the CSR values are both relatively low, suggesting that the multipass welds would have good resistance to weld metal liquation cracking. For austenitic stainless steels and Ni-based alloys, CSR values above 100°C are thought to be indicative of weld metals susceptible to weld metal liquation cracking (Refs. 26, 37).

If single-pass welding is being performed, then liquation cracking susceptibility in the HAZ is determined by the hot ductility of the base metal material. Plaut et al. have reviewed the hot ductility of wrought 304 stainless steel alloys tested at a strain rate of 6 s^{-1} (Ref. 44). They noted ductility loss in the range of 1250° to 1350°C for a range of stainless steel compositions. This was associated with a lack of grain boundary cohesion and the onset of liquation. Hot ductility of Type 304 is included in Fig. 9 for comparison with the Ni-Cu weld deposits (Ref. 44). The NDT temperature was not provided but appears to be in the range of 1350° to 1375°C if extrapolated to the zero ductility line. The CSR of Type 304 cannot be determined from on-heating curves alone. However, a comparison of Type 304 and the weld deposits provides some insight into mechanical performance. Clearly, the Type 304 wrought alloy has superior ductility to both types of weld deposits. Wrought 304 stainless steel tensile samples would likely contain a smaller equiaxed grain structure whereas the Ni-Cu deposits contain large columnar grains due to weld solidification. Larger grain sizes are typically associated with a decrease in ductility and toughness. This suggests that liquation cracking susceptibility would be low in single-pass dissimilar welds of this type because more ductility will always be available in Type 304 than in the weld deposit. This observation is made based on the on-heating hot ductility of Type 304 and the observation that Type 304 may also form ferrite at the grain boundaries in the HAZ, which further reduces susceptibility (Ref. 37).

Note that the Generation II-C on-heating and on-cooling hot ductility curves

Table 9 — Bulk Fume Compositions (wt-%) of Generation II and IV Welding Fumes Measured with EDS

Element	Generation II	Generation IV
O*	—	—
F*	—	—
Na	65.7	33.8
Al	—	21.5
Mg	0.4	2.5
Si	4.2	6.4
Cl	0.4	0.3
K	2.3	22.5
Ca	4.9	1.4
Ti	4.2	3.7
Cr	0.4	0.3
Mn	0.4	0.2
Fe	0.7	0.4
Ni	10.4	5.0
Cu	6.1	2.0

*Oxygen and fluorine were present but were not measured due to limitations of light element analysis with the EDS technique.

show a ductility dip in the temperature range from 850° to 1150°C. A similar observation was made in the on-heating curve of the Generation III deposit, where ductility was reduced in the range of approximately 800° to 1100°C. The on-cooling curve of the Generation III deposit also decreased at the lower temperatures. These temperature ranges correlate reasonably well with the solid-state cracking temperature ranges found during Varestraint testing of the weld deposits shown in Table 7. To further examine cracking susceptibility due to this ductility dip, and determine threshold strains necessary to induce DDC, samples of II-C and III-BW weld metal were subjected to the strain-to-fracture test.

Ductility Dip Cracking

It was not possible to determine threshold strains necessary to induce DDC during transvarestraint testing because the die blocks imposed fixed levels of strain (at 2% strain increments) to the weld metal during bending. The strain-to-fracture test is better suited to determine the threshold strains necessary to cause DDC because strain can be applied at smaller increasing increments until crack initiation occurs (Ref. 22). A test temperature of 950°C has been proposed as a suitable temperature for comparing DDC susceptibility of different alloys because it is typically the temperature where the minimum in the ductility trough occurs (Ref. 45). Therefore, this temperature was utilized to determine threshold strains necessary to induce DDC in Generation II and III-BW weld metals. Test samples were utilized with the configuration shown in Fig. 10A. Note that the base metal used for the samples was Type 304L. Weld deposits were made with Generation II and III consumables on one side of the sample during fabrication. Autogenous GTA spot welds were then placed on the weld deposit and on the Type 304L on the opposing side of the Generation III welds. Gauge marks were placed on the reduced center section. These were measured before and after testing to determine the average strain level imparted into the center section during the test. Note that strain is nonuniform across the gauge section due to the presence of a temperature gradient, which results in localized deformation. Samples of the configuration shown were heated to 950°C and strained to induce cracking, then carefully inspected under a binocular microscope after testing to determine the total number of cracks.

A comparison of cracking susceptibility at 950°C of Generation II-C and III deposits with other Ni-based filler metals (Ref. 46) and Type 304L is shown in Fig. 10B. The number of cracks observed on each specimen is listed. The plot shows that Generation III welds had a higher threshold strain than II-C deposits and is comparable to FM-82. The II-C deposits have a cracking susceptibility similar to FM-52. Type 304L had the highest threshold strain values and is generally considered very resistant to DDC. Nickel-based alloy FM-52 has a high DDC susceptibility in high-restraint, thick-section welds. It has the lowest cracking threshold of any of the weld metals included in Fig. 10. Note that the II-C deposit had similar threshold values as the FM-52 weld metal. Thus, it is likely that II-C would have a high cracking susceptibility in high-restraint welds. The III-BW weld metal appears to have a cracking threshold similar to FM-82 at intermediate temperatures. FM-82 is considered to have a better resistance to DDC than FM-52 (Ref. 47), therefore Generation III welds would be considered to have a similar cracking resistance in high-restraint welds as FM-82.

In addition to the threshold cracking strain, the transition to "massive cracking" has been established as an important indicator of cracking susceptibility (Ref. 46). Materials that transition from the threshold strain to massive cracking over a short strain interval were typically observed to have higher susceptibility to DDC. This was described as the strain where the number of cracks exceeded 50 in the spot weld or when they became too numerous to accurately count. Based on that criterion, the transition to massive cracking was not observed in Generation II-C or III deposits within the strain envelope of testing (less than 5% in Generation II-C and less than 7% in Generation III).

The Generation IV weld deposits exhibited higher grain boundary tortuosity due to grain boundary pinning by medium sized Ti(C,N) particles. Grain boundary pinning with medium-sized intergranular (Nb,Ti)C carbides and has been shown decrease DDC susceptibility in Ni-based weld deposits (Ref. 28). Other work showed that DDC susceptibility in Ni-based welds was decreased with an increase in intergranular carbide coverage, regardless of carbide type (Ref. 48). Therefore, future STF testing of Generation IV welds may reveal additional improvements in DDC resistance based on those observations.

Fume Characterization

A thorough analysis of fume produced by these consumables was necessary to ensure that Cr(VI) was sufficiently reduced to levels that would support their implementation. Welding fumes produced by the Generation II and Generation IV consumables were evaluated by performing fume generation rate measurements followed by composition analysis with EDS, and chemical analysis with XRD and visible absorption spectrophotometry to evaluate bulk fume phases and Cr(VI) content, respectively.

The measured FGR values are shown in Table 8 for E308-16, and Generation II and IV SMAW consumables. Welding parameters are also listed for each collection performed. Comparing the FGR measurements of the Generation II and IV consumables to values obtained for E308-16 shows the Generation II chromium-free electrodes have higher FGR values at similar heat inputs to the E308-16. The Generation IV consumables were tested at higher heat input conditions than Generation II because those different weld parameters were required to produce good quality weld deposits. The higher heat inputs used during Generation IV testing resulted in higher FGR values than the

E308-16 as well. However, the Ni-Cu consumables have lower FGR values than other flux-based processes such as the E308LT1-1 electrode used for flux cored arc welding (Ref. 49).

Bulk fume composition was measured with EDS as listed in Table 9. Note that some Cr was observed in the bulk fume, although this is much lower than levels observed in fumes of stainless steel welding consumables (Ref. 3). Phases in bulk welding fume were readily identified with XRD because the fumes collected on filters during FGR measurements were essentially in powder form. Particles analyzed with this technique varied across a broad size range based on observations with SEM. The XRD scan results are shown in Fig. 11A and B for the Generation II and IV bulk fumes, respectively. Note the different scales on the axes of the two spectra. Multiple phases were observed in both spectra; however, no phases were observed that contained Cr(VI) such as K_2CrO_4 or Na_2CrO_4 as previous evaluation of stainless steel welding fume has shown (Ref. 3).

The Cr(VI) concentrations in Generation II and Generation IV welding fumes are shown in Table 8. Measured Cr(VI) concentrations in the Generation II and IV welding fumes were reduced by two orders of magnitude compared to E308-16 tested at similar heat inputs. These concentrations represent an average value of all fume particle types and sizes as they were measured from bulk fume filters. The SMAW consumables developed during this work contained no measureable amounts of chromium in the flux coatings or core wires. Therefore, any Cr(VI) in the welding fume must have originated from the base plate because Type 304L contains approximately 18 wt-% Cr. It was not clear from the results obtained during XRD studies what phase(s) could have contained the Cr(VI). The very low concentrations of Cr(VI) as measured with colorimetric techniques (Table 8) indicate the compounds that give rise to its presence would be difficult to identify with diffraction because they would be present in such low concentrations. However, there were ample amounts of oxygen, potassium, and sodium within the bulk fume. Therefore, it is possible that Cr(VI) may have been detected as an oxide or chromate compound. Note that the Cr(VI) concentration in bulk fume scaled with heat input into the base metal as shown in Fig. 12 supporting the idea that complete elimination of chromate during arc welding is likely unavoidable because some vaporization of Cr from the molten weld pool will occur.

Consumable Applicability

The current study showed successful welding of Type 304L base metal during weldability evaluation of the consumables. The Generation III and IV consumables would likely have further success and application in welding other 300-series austenitic alloys. Some of the most widely used alloys in this series include Type 304, 316, 321, and 347, which are based on the 18Cr and 8-10Ni metallurgical system (Ref. 37). Weld fusion zones on these base metals would remain fully austenitic according to an analysis with the Schaeffler Diagram and assuming reasonable dilution levels by the consumables (Ref. 25). Susceptibility to solidification, ductility dip, and weld metal liquation cracking is expected to be similar to the current results based on this approximation alone. However, variations in minor alloying concentrations (such as C, Si, Ti, and Nb) in the other grades of base metal may alter cracking behavior to some extent. Heat-affected zone liquation cracking susceptibility would also be dominated by changes in base metal. In addition, the various stainless grades are used in a broad range of corrosive and high-temperature environments, which necessitates additional weld corrosion testing to determine performance in those environments. Further studies are required to substantiate applicability in a broader sense.

Summary and Conclusions

This study was performed to develop and evaluate a Cr-free welding consumable for the purpose of reducing Cr(VI) in the welding fume produced during joining of austenitic stainless steels. Various tests were performed to evaluate the weldability of a Ni-Cu-based consumable during joining of Type 304L austenitic stainless steel. These tests assessed the mechanical performance, corrosion characteristics, weld cracking susceptibility, and fume generation characteristics in comparison to data published elsewhere for conventional stainless steel welding consumables. Based on these tests, the following conclusions were made:

1. The final target composition for a bare wire consumable for GTAW (and potentially GMAW) was Ni-7.5Cu-1Ru-0.5Al-0.5Ti-0.02C. The final target composition for a SMAW core wire was Ni-7.5Cu-1Ru-0.5Al-4Ti-0.02C. Note that this core wire produced a weld deposit with a composition very close to that of the bare wire due to significant Ti loss in the arc.

2. Weld microstructures of GTAW and SMAW deposits consisted of a columnar austenitic grain structure with the presence of Ti(C,N) particles at solidification grain boundaries and cell and dendrite boundaries.

3. Welds deposited on Type 304L stainless steel using Generations II, III, and IV electrodes exhibited good mechanical properties. Tensile strengths of weld deposits exceeded minimum values required for E308-16 weld deposits. Elongation values of Generation III and IV deposits exceeded minimum values required for E308-16 weld deposits.

4. Electrochemical corrosion tests revealed that weld deposits met corrosion design criteria to avoid galvanic and localized corrosion in chloride environments.

5. Transvarestraint testing revealed that Generation II and III weld deposits had solidification cracking temperature range (SCTR) values of approximately 110°C. This is significantly higher than E308L weld metal (30°–40°C) but similar to other Ni-base weld deposits that exhibit moderate solidification cracking susceptibility.

6. Hot ductility testing revealed that the Generation II and III-BW deposits had low liquation cracking indexes as determined by the cracking susceptibility range (CSR) calculations. The CSR values were 33° and 54°C for Generation II and III weld deposits, respectively.

7. Generation III GTA weld deposits had better overall elevated temperature ductility than Generation II SMA weld deposits. Both deposits exhibited a ductility dip in the range of 800° to 1100°C.

8. Strain-to-fracture testing revealed that cracking threshold strains of Generation II (~2%) and III (~3%) weld metals were significantly lower than stainless steel alloys such as Type 304L, although threshold strain levels were comparable to other Ni-base filler metals.

9. Fume generation rates of the Generation II and IV consumables were higher than E308-16 at similar heat inputs but were lower than stainless steel flux cored welding consumables.

10. Cr(VI) bearing compounds were not detected when XRD was used to analyze the chemistry of bulk fume produced from the SMAW process.

11. Cr(VI) in the Generation II and IV welding fumes was reduced by two orders of magnitude compared to E308-16 tested at similar heat inputs. Complete elimination of Cr(VI) may be unavoidable because there will always be some vaporization of Cr from the molten surface during arc welding when there is some dilution of the Ni-Cu consumable by the stainless steel.

Acknowledgments

The authors wish to acknowledge the financial support of this project by the Strategic Environmental Research and Development Program (SERDP) Project #1415. Consumable production efforts of Special Metals, Euroweld Ltd., Electrode

Engineering, and Haynes International are greatly appreciated as is the weld process development assistance of Troy Paskell of WeldQC, Inc. Undergraduate lab assistants Adam Hope, Hadley Cluxton, Ben Sutton, Dan Saltzmann, and Pat Varga provided invaluable support during this work.

References

1. Castner, H. R., and Null, C. L. 1998. Chromium, nickel and manganese in shipyard welding fumes. *Welding Journal* 77(6): 223-s to 231-s.

2. Voitkevich, V. 1995. *Welding Fumes: Formation, Properties and Biological Effects*. Cambridge, Abington Publishing.

3. Kimura, S., Kobayashi, M., Godai, T., and Minato, S. 1979. Investigations on chromium in stainless steel welding fumes. *Welding Journal* 58(7): 195-s to 204-s.

4. Eagar, T. W., Sreekanthan, P., Jenkins, N. T., Krishna Murthy, G. G., Antonini, J. M., and Brain, J. D. 1998. Study of chromium in gas metal arc welding fume. *Trends in Welding Research: Proceedings of the 5th International Conference*. J. M. Vitek, S. A. David, J. Johnson, H. Smartt, and T. DebRoy, ASM International.

5. NIOSH. 1975. *Criteria for a Recommended Standard — Occupational Exposure to Chromium (VI)*. Washington, D.C.

6. OSHA. 2006. *Occupational Exposure to Hexavalent Chromium. Final Rule*. Washington, D.C.

7. Wallace, M. E., Fischbach, T., and Kovein, R. J. 1997. *In-depth survey report. Control technology assessment for the Welding Operations Boilermaker's National Apprenticeship Training School*. Kansas City, Kan., Occupational Safety and Health Administration.

8. Fiore, S. R. 2006. Reducing exposure to hexavalent chromium in welding fumes. *Welding Journal* 85(8): 38 to 42.

9. Dennis, J. H., French, M. J., Hewitt, P. J., Mortazavi, S. B., and Redding, C. A. J. 2002. Control of occupational exposure to hexavalent chromium and ozone in tubular wire arc-welding processes by replacement of potassium by lithium or by addition of zinc. *The Annals of Occupational Hygiene* 46(1): 33–42.

10. Dennis, J. H., French, M. J., Hewitt, P. J., Mortazavi, S. B., and Redding, C. A. J. 2002. Control of exposure to hexavalent chromium and ozone in gas metal arc welding of stainless steels by use of a secondary shield gas. *The Annals of Occupational Hygiene* 46(1): 43–48.

11. Kim, Y. H., Frankel, G. S., Lippold, J. C., and Guaytima, G. 2006. Development of a chromium-free consumable for austenitic stainless steels — Part 1: Monel (Alloy 400) filler metal. *Corrosion* 62(1): 44–53.

12. Kim, Y. H., Frankel, G. S., and Lippold, J. C. 2006. Development of a chromium-free consumable for austenitic stainless steels — Part 2: Optimization of alloy composition based on corrosion behavior. *Corrosion* 62(2): 109–120.

13. Kim, Y. H., Frankel, G. S., and Lippold, J. C. 2006. Development of a chromium-free consumable for austenitic stainless steels: Effect of dilution and the behavior of bead-on-plate welds. *ISIJ International* 46(5): 698 to 704.

14. Kim, Y. H. 2005. Chromium-free consumable for welding stainless steel: corrosion perspective. PhD dissertation. The Ohio State University, Columbus, Ohio.

15. Guaytima, G. 2004. A study of Ni-Cu weld metals for joining austenitic stainless steels. MS thesis. The Ohio State University, Columbus, Ohio.

16. Connor, L. ed. 1987. Welding technology. *Welding Handbook*, Vol. 1, Eighth Edition, p. 111. Miami, Fla.: American Welding Society.

17. Sowards, J. W. 2009. Development of a chromium-free consumable for joining stainless steels. PhD dissertation. The Ohio State University, Columbus, Ohio.

18. Liang, D., Sowards, J. W., Frankel, G. S., Alexandrov, B. T., and Lippold, J. C. 2010. A corrosion study of nickel-copper and nickel-copper-palladium welding filler metals. *In Press: Materials and Corrosion*. DOI: 10.1002/maco.200905583.

19. Liang, D., Sowards, J. W., Frankel, G. S., Alexandrov, B. T., and Lippold, J. C. 2010. Corrosion resistance of welds in Type 304L stainless steel made with a nickel-copper-ruthenium welding consumable. *Corrosion Science* 52(7): 2439–2451.

20. AWS B4.0: 1998, *Standard Methods for Mechanical Testing of Welds*. American Welding Society, Miami, Fla.

21. ASTM E8, *Standard Test Methods for Tension Testing of Metallic Materials*. 2004. ASTM, Philadelphia, Pa.

22. Nissley, N. E., and Lippold, J. C. 2003. Development of the strain-to-fracture test. *Welding Journal* 82(12): 355-s to 364-s.

23. AWS F1.2: 1999, *Laboratory Method for Measuring Fume Generation Rates and Total Fume Emission of Welding and Allied Processes*. American Welding Society, Miami, Fla.

24. Sowards, J. W., Ramirez, A. J., Lippold, J. C., and Dickinson, D. W. 2008. Characterization procedure for the analysis of arc welding fume. *Welding Journal* 87(3): 76-s to 83-s.

25. Schaeffler, A. L. 1948. Welding dissimilar metals with stainless electrodes. *Iron Age* 162: 72.

26. DuPont, J. N., Lippold, J. C., and Kiser, S. D. 2009. *Welding Metallurgy and Weldability of Nickel-base Alloys*. Hoboken, N.J.: John Wiley & Sons, Inc.

27. Pokhodnya, I. K., Gorpenyuk, V. N., Milichenko, S. S., Ponomarev, V. E., Starodubtsev, L. V., Shvachko, V. I., and Yavdoshchin, I.R. 1991. *Metallurgy of Arc Welding*. Cambridge, Riecansky Science Publishing Co.

28. Ramirez, A. J., and Lippold, J. C. 2004. High temperature behavior of Ni-base weld metal — Part II — Insight into the mechanism for ductility dip cracking. *Materials Science and Engineering A-Structural Materials Properties Microstructure and Processing* 380(1–2): 245–258.

29. Matsuda, F., Nakagawa, H., and Zhang, Y.-C. 1985. Study on metallurgical factors causing ductility-dip crack in weld metal of Invar (Report III). *Quarterly Journal of the Japan Welding Society* 4(1): 125 to 130.

30. Cui, Y., and Lundin, C. D. 2005. Effect of microfissures on mechanical properties of 308L austenitic stainless steel weld metals. *Journal of Materials Science* 40(5): 1281–1283.

31. *ASM Metals Reference Book*, Third Edition. 1993. Materials Park, Ohio: ASM International.

32. A5.4, *Specification for Stainless Steel Electrodes for Shielded Metal Arc Welding*. 1992. Miami, Fla., American Welding Society.

33. Szarska-Smialowska, S. 2005. *Pitting Corrosion of Metals*. Houston: NACE Press.

34. Copson, H. R. 1959. *Physical Metallurgy of Stress Corrosion Fracture*. New York: Interscience.

35. Lippold, J. C., Sowards, J. W., Murray, G. M., Alexandrov, B. T., and Ramirez, A. J. 2008. Weld solidification cracking in solid-solution strengthened Ni-base filler metals. *Hot Cracking Phenomena in Welds II*: 147–170.

36. DuPont, J. N., Michael, J. R., and Newbury, B. D. 1999. Welding metallurgy of Alloy HR-160 (R). *Welding Journal* 78(12): 408-s to 415-s.

37. Lippold, J. C., and Kotecki, D. J. 2005. *Welding Metallurgy and Weldability of Stainless Steels*. Hoboken, N.J.: John Wiley & Sons, Inc.

38. Kou, S. 2003. *Welding Metallurgy*, 2nd Ed. Hoboken, N.J.: John Wiley & Sons, Inc.

39. Kiser, S. D. 1988. Welding high-nickel alloys: different but not difficult. *Welding Journal* 67(10): 55–57.

40. Monel Welding Electrode 190 (nickel-base alloy). 1985. *Alloy Digest* (2): 1, 2.

41. Takalo, T., Suutala, N., and Moisio, T. 1979. Austenitic solidification mode in austenitic stainless steel welds. *Metallurgical Transactions A* 10(8): 1173–1181.

42. Noecker, F. F., and DuPont, J. N. 2007. Microstructural development and solidification cracking susceptibility of Cu deposits on steel: Part II — use of a Ni interlayer. *Journal of Materials Science* 42(2): 510 to 521.

43. Lin, W., Baeslack, W. A., and Lippold, J. C. 1990. Hot-ductility testing of high-strength low-expansion superalloys. *Proceedings of the Conference on Recent Trends in Welding Science and Technology*. Eds. S. A. David and J. M. Vitek, pp. 609 to 614. ASM International.

44. Plaut, R. L., Herrera, C., Escriba, D. M., Rios, P. R., and Padihla, A. F. 2007. A short review on wrought austenitic stainless steels at high temperatures: processing, microstructure, properties and performance. *Materials Research* 10(4): 453 to 460.

45. Ramirez, A. J., and Lippold, J. C. 2004. High temperature behavior of Ni-base weld metal Part I. Ductility and microstructural characterization. *Materials Science and Engineering A* 380(1-2): 259–271.

46. Nissley, N. E. 2006. Intermediate temperature grain boundary embrittlement in nickel-base weld metals. PhD dissertation. The Ohio State University, Columbus, Ohio.

47. Collins, M. G., and Lippold, J. C. 2003. An investigation of ductility dip cracking in nickel-based filler materials — Part I. *Welding Journal* 82(10): 288-s to 295-s.

48. Noecker, F. F., and DuPont, J. N. 2009. Metallurgical investigation into ductility dip cracking in Ni-based alloys: Part II. *Welding Journal* 88(3): 62-s to 77-s.

49. Gonser, M. 2006. Characterization of welding aerosol from a series of welding consumables. MS thesis. The Ohio State University, Columbus, Ohio.